Pergamon

PII: S0301-9322(96)00065-1

Int. J. Multiphase Flow Vol. 23, No. 2, pp. 337–355, 1997

0301-9322/97 $17.00 + 0.00

DISPERSION AND POLYDISPERSITY OF DROPLETS IN STATIONARY ISOTROPIC TURBULENCE

F. MASHAYEK, F. A. JABERI, R. S. MILLER and P. GIVI

Department of Mechanical and Aerospace Engineering, State University of New York at Buffalo, Buffalo, NY 14260-4400, U.S.A.

(Received 12 July 1995; in revised form 22 August 1996)

Abstract—A detailed parametric study is conducted of dispersion and polydispersity of liquid drops in stationary isotropic turbulence via direct numerical simulation. It is assumed that the flow is very dilute so that the effect of particles on the carrier fluid is negligible (one-way coupling). Both non-evaporating and evaporating drops are simulated; in the latter both constant and variable rates of evaporation are considered. The simulations of non-evaporating drops are used to validate the numerical methodology and to assess the effects of the particle time constant and the drift velocity on the particle velocity autocorrelation, turbulence intensity and diffusivity. The simulated results are also used to appraise the performance of some of the available theoretical models for particle dispersion in stationary isotropic turbulence. The effects of the initial drop time constant, the initial evaporation rate, and the drop Schmidt number on the probability density function (pdf) of the drop size are studied. It is found that, after an initial transient period the pdf of the drop size becomes nearly Gaussian. However, the pdf deviates from Gaussian as the mean drop time constant becomes very small. The extent of this deviation depends on the evaporation rate. The effect of the initial spray size on the pdf is also studied and it is shown that as the spray size increases, the interaction between the spray and large scale turbulence structures influences the pdf. The effect of the initial size distribution on the pdf is also investigated by varying the initial standard deviation. Both Gaussian and double-delta initial drop size pdfs are considered. In the latter it is shown that a transition to Gaussian is possible provided that the initial mean drop time constant is large and/or the initial standard deviation of the drop diameter is small. © 1997 Elsevier Science Ltd. All rights reserved.

Key Words: direct numerical simulation, isotropic turbulence, particle dispersion, polydispersity, evaporating drops, drop size distribution

1. INTRODUCTION

Dispersion of heavy particles in turbulent flows has been the subject of numerous investigations in recent years due to its applications in various aspects of technology (Eaton and Fessler 1994; McLauglin 1994). One of the early theoretical studies of particle dispersion in turbulence is due to Tchen (1947) who derives relations for the particle diffusion coefficient under the assumption that the particle's neighbouring fluid does not change in the course of its motion. Yudine (1959) clarifies the consequences of this assumption by analyzing the motion of heavy particles in the presence of gravity and shows that as the heavy particle is transported under the influence of the external body force, its trajectory crosses that of the neighbouring fluid particle which is not affected by the gravity. This is referred to as the "crossing trajectories effect". Csanady (1963) points out the "continuity effect" which is associated with the crossing trajectories effect in the presence of gravity, and results in the reduction of the velocity autocorrelation in directions normal to the gravity direction in comparison to that in the gravity direction. Further relations for the velocity autocorrelation, the diffusion coefficient and the turbulence intensity of particle loaded turbulent flows are obtained by assuming either the fluid velocity autocorrelation along the particle trajectory (Reeks 1971; Pismen and Nir 1978) or the fluid spectral density function (Mei *et al.* 1991).

Experimental studies of particle dispersion in turbulent flow are pioneered by Snyder and Lumley (1971) who investigate dispersion characteristics of solid particles. They find that the particle inertia decreases its turbulence intensity in comparison to the fluid turbulence intensity. Wells and Stock (1983) study the effects of crossing trajectories in a homogeneous decaying turbulent flow. Using an electric field, they succeed to eliminate or enhance the effects of gravity, and indicate that the long time asymptotic particle diffusion coefficient is primarily affected by the drift velocity and that

the particle time constant is mostly effective in modifying the particle turbulence intensity. The experimental and numerical results of Wen *et al.* (1992) in shear flows show that particles with large response times are centrifuged toward the outer edges of the vortex structures resulting in higher particle diffusivity coefficients.

Experimental studies of evaporating drops are somewhat limited in comparison to those of solid particle dispersion. Previous studies have been mostly directed to assess the performance of turbulence models in multiphase flows. Shearer *et al.* (1979) conduct experiments on axisymmetric particle-laden jet flows to appraise the performance of a locally homogeneous flow model for evaporating sprays. A somewhat similar experiment is conducted by Solomon *et al.* (1984) with different loading ratios. Further laboratory and numerical experiments are conducted by Nguyen *et al.* (1991) who investigate the effects of the interactions among the drops on the drag force and the evaporation rate.

The important role of the small scales of the carrier phase in the dynamics of heavy particles has motivated the use of direct numerical simulation (DNS). The implementation of DNS in two-phase flows is pioneered by Riley and Patterson (1974) to investigate particle dispersion in decaying isotropic turbulence. Using a low resolution simulation (32^3 grid points) and a relatively small number of particles (432), they find that an increase of the particle inertia increases the velocity autocorrelation. McLaughlin (1989) simulates particle deposition in a channel flow and shows the tendency of particles to accumulate in the viscous sublayer. Squires and Eaton (1990, 1991a, 1991b) simulate both stationary and decaying turbulence fields with one- and two-way coupling. The results show the increase of the eddy diffusivity of heavy particles over that of the fluid particle for cases with one-way coupling. In the cases with two-way coupling they find that the fraction of energy at high wavenumbers of the spatial energy spectrum of turbulence increases relative to that at low wavenumbers as the mass loading ratio is increased. They also find that large particles tend to collect preferentially in regions of low vorticity and high strain. This is also true for the cases with one-way coupling. Elghobashi and Truesdell (1992, 1993); Truesdell and Elghobashi (1994) conduct similar studies. They consider the full equation for the particle motion and show that the Stokes drag is of primary importance for large density ratios. In the presence of both gravity and two-way coupling they show that energy is transferred from the gravity direction to other directions by the pressure–strain correlation. The settling velocity of heavy particles in isotropic turbulence is studied by Wang and Maxey (1993) for different particle time constants and drift velocities. The results show an increase of the settling velocity for all cases. The maximum increase in settling velocity is obtained when both the particle time constant and the drift velocity are comparable to the Kolmogorov scales.

This paper deals with the problem of dispersion and polydispersity of evaporating drops in an isotropic turbulent flow via DNS. The DNS generated data are statistically analyzed to extract important physical information pertaining to turbulent dispersion of evaporating drops. While the polydispersity phenomenon caused by evaporation is the primary subject of this study, some issues pertaining to dispersion of nonevaporating drops (solid particles) are also considered. In this consideration, a detailed parametric study is conducted and the results are comparatively assessed via existing analytical, experimental and, if applicable, DNS results. This assessment is very useful for validations of our computational methodology and for the parameterization in the evaporating drops simulations. In section 2 the problem formulation and numerical technique are described, in section 3 the DNS results are analyzed; the summary along with concluding remarks are furnished in section 4.

2. PROBLEM FORMULATION AND NUMERICAL TECHNIQUE

Since this is the first attempt in DNS of the evaporating drop dispersion in turbulent flows, the problem is formulated based on models and correlations which are well established. The implementation of these models requires several simplifying assumptions; these are discussed in this section within the framework of the mathematical formulation. We consider motion of spherical particles in an incompressible and isotropic turbulent flow. It is assumed that the dispersed phase is very dilute, thus the effect of particles on the carrier fluid is negligible. The momentum equation for each particle is considered in the Lagrangian frame of reference. In general, this equation

contains the Stokes drag, the Basset force, the force due to fluid pressure gradient, the inertia force of added mass, and gravity (Maxey and Riley 1983). However, the results of several previous studies, e.g. Elghobashi and Truesdell (1992), indicate that if the ratio of the density of the particle to the density of the carrier fluid is large, the Stokes drag and the gravity forces are dominant and the other forces can be assumed negligible. With this assumption the momentum equation for a single particle is expressed as:

$$\frac{\mathrm{d}\mathbf{v}}{\mathrm{d}t} = \frac{18\mu}{\rho_p d_p^2}(\mathbf{u} - \mathbf{v}) + g\mathbf{e}, \tag{1}$$

$$\frac{\mathrm{d}\mathbf{X}}{\mathrm{d}t} = \mathbf{v}, \tag{2}$$

where $\mathbf{u}$ and $\mathbf{v}$ (boldface indicates vector) denote the fluid velocity at the particle location and the particle velocity, respectively; t is time, $\mathbf{X}$ is the center position of the particle, $\mathbf{e}$ is the unit vector in the gravity direction, g is the gravity constant; ρ_p and d_p denote the particle density and diameter, respectively; and μ is the fluid viscosity. All of the variables are normalized by reference scales of length, L_0, velocity, U_0, and density, ρ_0. The length scale is conveniently chosen such that the normalized size of the simulation box is 2π and the velocity scale is found from the box Reynolds number, $\mathrm{Re}_0 = (\rho_0 U_0 L_0/\mu)$. The fluid density is used as the scale for density.

In the simulations of non-evaporating (solid sphere) particles, the particle diameter remains constant. For the evaporating particles, the rate of diameter reduction is modeled by the d^2-law (Strehlow 1985):

$$d_p^2 = d_{p0}^2 - \kappa t, \tag{3}$$

where d_{p0} is the initial diameter of the particle and the depletion rate is given by $\kappa = 8\Gamma \ln(1 + B_M)C_{Re}$, where Γ is the mass diffusivity coefficient and B_M is the transfer number (Spalding 1953). The parameter C_{Re} is a correction factor to account for the convective effects (Ranz and Marshall 1952):

$$C_{Re} = 1 + 0.3\mathrm{Re}_p^{0.5}\mathrm{Sc}_p^{0.333}, \tag{4}$$

with Re_p and Sc_p representing the particle Reynolds and Schmidt numbers, respectively. It is assumed that the flow is isothermal and that evaporation is due to a constant temperature difference between the drop and the fluid. This model is in accord with that of several laboratory experiments (e.g. Shearer *et al.* 1979). In a dilute flow, the ratio of the mass of the particle to the mass of the carrier fluid is very small and it is assumed that all the particles are in contact with the carrier fluid during evaporation. Therefore, the variation of κ is only due to C_{Re}. The "particle time constant" (τ_p) is defined by:

$$\tau_p(t) = \frac{\rho_p d_p^2}{18\mu} = \tau_{p0} - \tau_e t, \tag{5}$$

where $\tau_{p0} = (\rho_p d_{p0}^2/18\mu)$ denotes the initial particle time constant, and:

$$\tau_e = C_{Re}\tau_{e0}, \quad \tau_{e0} = \frac{4\rho_p\Gamma}{9\mu}\ln(1 + B_M). \tag{6}$$

By introducing a drift velocity, $v_{dr} = \tau_{p0}g$, [1] is expressed as:

$$\frac{\mathrm{d}\boldsymbol{v}}{\mathrm{d}t} = \frac{1}{\tau_p}(\mathbf{u} - \mathbf{v}) + \frac{1}{\tau_{p0}}v_{dr}\mathbf{e}. \tag{7}$$

The particle Reynolds number is defined as: $\mathrm{Re}_p = (\rho_f d_p|\mathbf{u} - \mathbf{v}|)/\mu$ with ρ_f denoting the carrier fluid density. Following Wang and Maxey (1993) the Reynolds number is related to the Kolmogorov time (τ_k) and velocity (v_k) scales with $\nu = \tau_k v_k^2$, where $\nu = \mu/\rho_f$ is the fluid kinematic viscosity:

$$\mathrm{Re}_p = \left(\frac{18\tau_p}{\nu\rho_p/\rho_f}\right)^{1/2}|\mathbf{u} - \mathbf{v}| = 4.243\left(\frac{\rho_f}{\rho_p}\right)^{1/2}\left(\frac{\tau_p}{\tau_k}\right)^{1/2}\frac{|\mathbf{u} - \mathbf{v}|}{v_k}. \tag{8}$$

The density ratio is kept constant ($\rho_f/\rho_p = 10^{-3}$) in all the simulations.

With the assumption of dilute particles, the Eulerian equations governing the carrier gas transport are solved independently to determine the **u**-field. With the assumptions of incompressible, isothermal flows this field influences dispersion, but not the other way around (i.e. one-way coupling). Also, the possible corrections to the convective effects in the drop evaporation due to flow unsteadiness, and the modifications of the drag force due to drop evaporation are not considered. The DNS of the carrier fluid is based on a spectral collocation scheme involving Fourier basis functions (Givi and Madnia 1993). The turbulent flow is assumed isotropic with triply periodic boundary conditions, and is forced at low wavenumbers to maintain a stationary (non-decaying) turbulent field (Givi 1989). Equations [1] and [2] are integrated in time using a second order accurate Runge–Kutta numerical scheme. The fluid velocity at the particle location is evaluated by a fourth order accurate Lagrange four point interpolation scheme.

3. RESULTS

Table 1 provides a listing of the flow parameters considered in the simulations. In this table, Re_λ is the flow Reynolds number based on the Taylor length scale (λ) and the root mean square of the flow velocity (u'), k_{max} denotes the highest resolved wavenumber after deailiasing, η represents the Kolmogorov length scale, u' is the root mean square of fluctuating velocity, and l is the integral length scale determined from the energy spectrum $E(k)$:

$$l = \frac{\pi}{2u'^2}\int_0^\infty \frac{E(k)}{k}\,\mathrm{d}k.$$

The parameters listed in table 1 are used in the simulations of both non-evaporating and evaporating drops. All the simulations are performed on 64^3 collocation points. In order to determine the appropriate number of particles, some preliminary simulations are conducted with 16^3, 21^3, and 25^3 particles. In agreement with the results of similar tests performed by Elghobashi and Truesdell (1992) it is found that 21^3 particles provide sufficient accuracy. In the simulations of the non-evaporating and constant rate evaporating particles, 21^3 particles are tracked. In the simulations of variable rate evaporating particles 25^3 particles are considered. In the discussion below $\langle\langle\cdot\rangle\rangle$ and $\langle\cdot\rangle$ denote the Lagrangian and Eulerian average values, respectively. The time averaged quantity is denoted by an overbar. In the presentation of the results, time is normalized with the eddy turn over time, l/u'.

3.1. *Dispersion of non-evaporating particles*

The purpose of simulations considered in this subsection is threefold: (1) to validate our present computational methodology by comparison with previous DNS results, (2) to appraise the performance of some of the recent models via comparative assessment with present DNS results, and (3) to identify the range of parameters in the evaporating drop simulations (discussed below) and to compare present results with those in the presence of evaporation.

In the simulations here, the particles are initially distributed uniformly within the box and are released with the same velocity as that of the local fluid particle. In order to obtain stationary conditions, the particles are allowed to interact with the flow for more than three eddy turnover times before data are extracted for statistical analysis. A measure of stationarity is the temporal variation of $\langle\langle Re_p\rangle\rangle$ as shown in figure 1 for four different τ_p values with zero gravity. This figure shows that a nearly stationary level is reached after an initial steep increase with a noticeable overshoot for cases with $\tau_p > \tau_k$. The magnitude of $\langle\langle Re_p\rangle\rangle$ at the stationary condition increases with the increase of τ_p due to the larger slip velocity experienced by heavier particles.

Table 1. Flow parameters used in the simulations

Re_λ	ηk_{max}	τ_k	ν_k	u'	l
41	1.41	8.229	5.72×10^{-3}	0.019	1.068

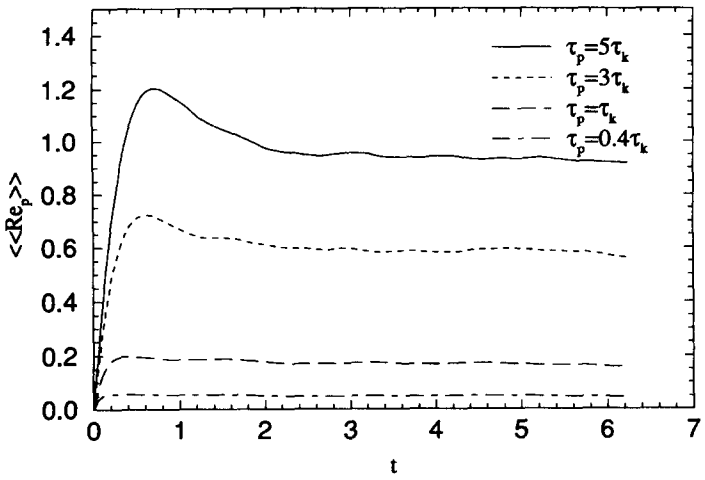

Figure 1. Temporal variation of $\langle\langle Re_p \rangle\rangle$ for different values of the particle time constant.

It is useful to consider the Fourier transform of [7] (Chao 1964). This transform in time for $\mathbf{w} = \mathbf{v} - v_{dr}\mathbf{e}$ yields:

$$\frac{E_{ij}^{p}(\omega)}{E_{ij}^{f}(\omega)} = \frac{1}{1 + \tau_p^2\omega^2}, \qquad [9]$$

where the spectral density function of the fluid velocity evaluated on the particle trajectory is $E_{ij}^{f}(\omega) = \langle\langle \hat{u}_i(\omega)\hat{u}_j^*(\omega)\rangle\rangle$ ($\hat{}$ indicates the variable in the Fourier space, * denotes complex conjugate, and ω is the frequency), and $E_{ij}^{p}(\omega) = \langle\langle \hat{w}_i(\omega)\hat{w}_j^*(\omega)\rangle\rangle$ is the spectral density function of the particle velocity. The decrease of the ratio of $E_{ij}^{p}(\omega)$ to $E_{ij}^{f}(\omega)$ with the increase of τ_p indicates that heavy particles have a less tendency to adjust to the flow fluctuations. Equations [9] also shows that $E_{ij}^{p}(\omega)$ deviates more from $E_{ij}^{f}(\omega)$ as ω increases. Therefore, the ability of the heavy particle to follow the fluid fluctuations decreases at high frequencies.

Mei *et al.* (1991) obtain a solution for the particle turbulence intensity $\langle\langle w^2 \rangle\rangle$, and the particle diffusion coefficient, ϵ^p, by assuming the form of the spectral density function as proposed by Kraichnan (1970). They consider contributions of all the forces acting on the particle but suggest that only the Stokes drag and the Basset forces need to be retained. Their final results for cases in which the Basset force is neglected, are compared with our DNS data as will be presented below. However, it should be mentioned that although Mei *et al.* (1991) consider a wide range of τ_p and v_{dr} values, our DNS results indicate (not shown) that for $\tau_p > 5\tau_k$ and $v_{dr} > 5v_k$ the particle Reynolds number becomes considerably larger than unity and is beyond the range of validity of the Stokes drag. Therefore, we limit our parameter range to $\tau_p \leqslant 5\tau_k$ and $v_{dr} \leqslant 5v_k$.

Figure 2 shows the particle velocity autocorrelation for four particle time constants at different drift velocities. The autocorrelation of the fluid particle ($\tau_p = 0$) is also shown for comparison. The velocity autocorrelation is defined as:

$$R_{\alpha\alpha}^{p}(t) = \frac{\langle\langle w_\alpha(0)w_\alpha(t)\rangle\rangle}{\langle\langle w_\alpha^2(0)\rangle\rangle} \quad \alpha = 1,2,3 \qquad [10]$$

where α refers to the coordinate direction (with no summation over repeated Greek indices). In order to reduce the effect of anisotropy, the autocorrelations are calculated by averaging over the three directions. These averaged autocorrelations are denoted by R^p (no subscripts). In cases with a non-zero drift velocity, three different simulations are performed for each case (using the same velocity field for the fluid) with the gravity direction changing for each simulation. Therefore, the velocity autocorrelation in the gravity direction is evaluated by averaging over the three gravity directions, and those in no-gravity directions are averaged over six other directions considered in three simulations. Inspection of figure 2 reveals that variations of the particle velocity autocorrelation with the particle time constant and the drift velocity are in accord with previous observations (e.g. Csanady 1963; Wells and Stock 1983).

The variations of the particle turbulence intensity $\overline{\langle\langle w^2 \rangle\rangle}$ (normalized by the fluid turbulence intensity $\langle u^2 \rangle$) due to the particle time constant and the drift velocity are shown in figure 3 and are compared with theoretical results of Mei *et al.* (1991). The temporal averages are evaluated by data sampling over more than three eddy turnover times. This figure indicates that, as the particle time constant is increased the particle turbulence intensity is reduced. In other words, the increase of the particle time constant decreases the drop tendency to follow the fluid motion. As τ_p is decreased, $\overline{\langle\langle w^2 \rangle\rangle}/\overline{\langle u^2 \rangle}$ approaches unity. This is expected since $w_i = u_i$ for $\tau_p = 0$. Although we have not performed simulations with $\tau_p < 0.4\tau_k$, the results suggest the existence of a plateau for $v_{dr} = 0$ near $\tau_p = 0$. This is also observed in the results of Mei *et al.* (1991).

Comparing the values of $\overline{\langle\langle w^2 \rangle\rangle}/\overline{\langle u^2 \rangle}$ in the no-gravity direction for $v_{dr} = v_k$ and $v_{dr} = 5v_k$ with those obtained for $v_{dr} = 0$ indicates the decrease of the particle turbulence intensity with the increase of gravity. Particles moving in the presence of a gravity field have a shorter time to interact with the instantaneous surrounding fluid particles in comparison with the particles moving in the zero

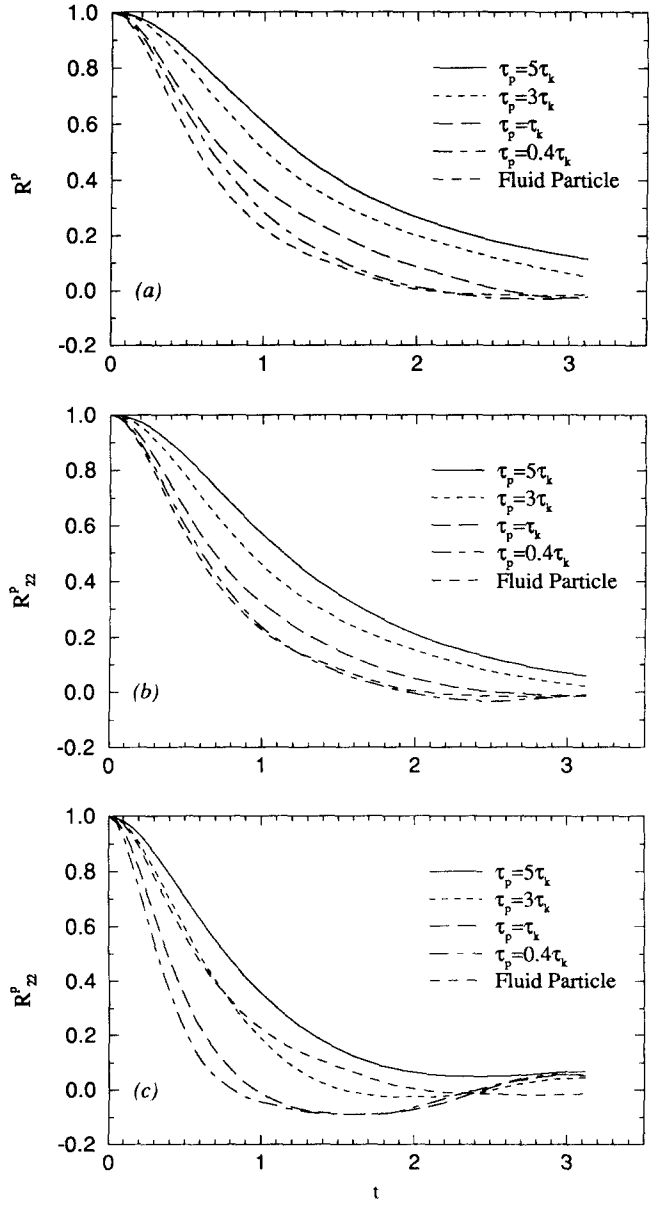

Figure 2. Particle velocity autocorrelations in the direction normal to the gravity direction. (a) $v_{dr} = 0$, (b) $v_{dr} = v_k$, and (c) $v_{dr} = 5v_k$.

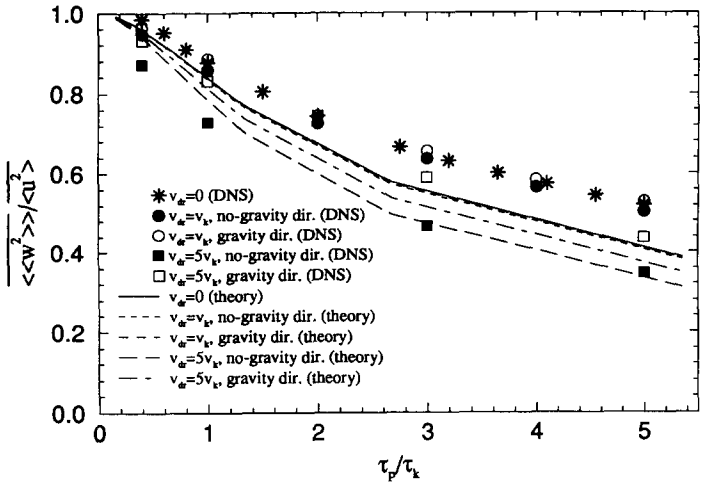

Figure 3. Variation of the particle turbulence intensity normalized with the fluid turbulence intensity with particle time constant.

gravity environment. However, as the particle time constant approaches zero, $\overline{\langle\langle w^2\rangle\rangle}/\overline{\langle u^2\rangle}$ approaches unity for all the v_{dr} values. This is due to the increase of particles' tendency to follow the fluid particle motion as the particle time constant is decreased. Figure 3 also shows that at a given particle time constant the turbulence intensity of the particle in the gravity direction is larger than that in the direction normal to the gravity direction.

Of central importance in the study of turbulent particle dispersion is the particle diffusion coefficient defined as (Hinze 1975):

$$\epsilon^{p}_{\alpha\alpha}(t) = \frac{1}{2}\frac{d}{dt}\langle\langle X^2_\alpha(t)\rangle\rangle \quad \alpha = 1,2,3. \tag{11}$$

For stationary particles, this coefficient is related to the velocity autocorrelation by:

$$\epsilon^{p}_{\alpha\alpha}(t) = \langle\langle w^2_\alpha(0)\rangle\rangle \int_0^t R^{p}_{\alpha\alpha}(\tau)d\tau = \int_0^t \langle\langle w_\alpha(0)w_\alpha(\tau)\rangle\rangle d\tau. \tag{12}$$

The fluid particle diffusion coefficient $\epsilon^{f}_{\alpha\alpha}$, is defined similarly by replacing w_α with u_α in [12]. Figure 4 shows the variations of the "asymptotic diffusion coefficient", $\epsilon^{p}(\infty)$ with the particle time constant and the drift velocity. Equation [12] is used for the determination of ϵ^{p} and the results are averaged in the three directions. Several observations are made from this figure: (i) in the absence of gravity ($v_{dr} = 0$) a peak is observed near $\tau_p = \tau_k$. The DNS results of Squires and Eaton (1991a) in stationary turbulence also show a similar behavior. However, this is in contrast to the analytical results of Pismen and Nir (1978) and Mei *et al.* (1991) which show a monotonic variation for $\epsilon^{p}(\infty)$ with τ_p. Squires and Eaton (1991a) attribute the difference between the analytical and DNS results to the sensitivity of the numerical results to the sample of large scale motions in forced turbulence; (ii) the increase of the drift velocity decreases the particle diffusion coefficient in both parallel and normal directions to the gravity direction. This behavior is also predicted by the models of Csanady (1963) and Mei *et al.* (1991); (iii) the diffusion coefficients are larger in the gravity direction than those in the direction normal to the gravity direction; however, the difference decreases with the increase of τ_p; (iv) in agreement with the experimental results of Wells and Stock (1983) the asymptotic diffusion coefficients are more sensitive to the drift velocity than to the particle time constant.

Figure 4 also indicates that as the particle time constant approaches zero, for a constant drift velocity, the particle diffusion coefficient does not equate that of the massless fluid particle. This is in contrast to the behavior of the particle turbulence intensity which approaches the fluid turbulence intensity as $\tau_p \to 0$ (cf. figure 3). A decrease of the particle time constant, while the magnitude of the drift velocity is kept fixed, corresponds to an increase of the gravity coefficient.

Very small particles have small relative velocities and are capable of responding to local fluid fluctuations instantaneously. This results in the adjustment of the particle turbulence intensity to that of the fluid. However, since the effect of gravity on the carrier phase is neglected, by having a finite drift velocity the particles move quickly through the vortical structures. This decreases the particle velocity autocorrelation and therefore the diffusion coefficient.

3.2. *Polydispersity of evaporating particles*

One of the major differences between non-evaporating and evaporating particle dispersion phenomena is the lack of a stationary condition in the latter. When evaporating, the magnitude of τ_p continuously decreases with time; thus the momentum transfer between the particle and the surrounding fluid is in a transient condition. At a constant gravity level, the problem of evaporating particle dispersion is parametrized by: the initial particle time constant (τ_{p0}), the initial rate of evaporation (τ_{e0}), and the particle Schmidt number (Sc_p). In addition, due to the intrinsic non-stationary nature of the problem, the effects of initial conditions should also be considered. In the following simulations, the largest evaporation rate is chosen such that the velocity autocorrelation becomes close to zero by the time $\tau_p = 0.1\tau_{p0}$ (about 3.1 eddy turnover times). Very low τ_p values are not considered to avoid excessive computational requirements for particle tracking. Therefore, we set $\tau_{e0} = 0.9\tau_{ec}/3.1 = 0.29\tau_{ec}$ where τ_{ec} is introduced to relate the evaporation rate to the initial particle time constant.

First, we consider cases with constant rate of evaporation in which the decay of τ_p is the same for all particles. These cases are exemplified by neglecting the nonlinear term in [4], i.e. $C_{Re} = 1$. Figure 5 shows the velocity autocorrelation for evaporating particles. The autocorrelation of non-evaporating particles ($\tau_{ec} = 0$) is also presented for comparison. The initial position and velocity of the particles are taken from the simulations of nonevaporating particles at the same particle time constant. Therefore, the particles are stationary at time $t = 0$ before the onset of

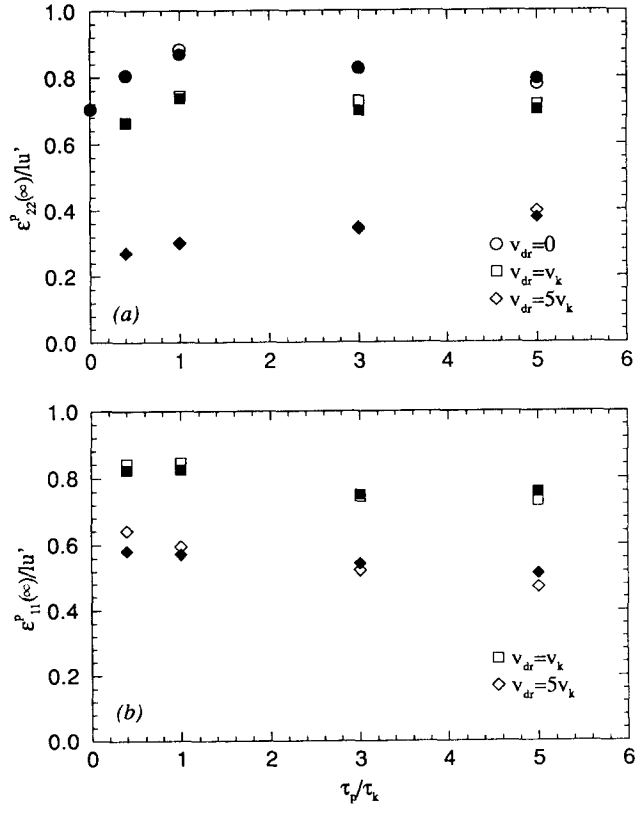

Figure 4. Variation of the diffusion coefficient for the heavy particle (hollow symbols) and the surrounding fluid particle (solid symbols) with the particle time constant: (a) in the direction normal to the gravity direction, (b) in the gravity direction.

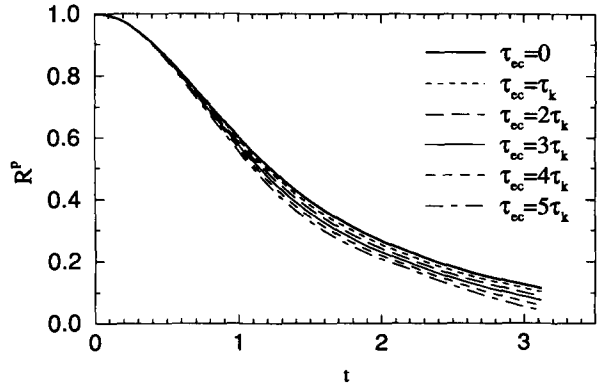

Figure 5. The velocity autocorrelation for the heavy particle at various evaporation rates for $\tau_{p0} = 5\tau_k$.

evaporation. The initial particle time constant is $\tau_{p0} = 5\tau_k$, and with a rate of evaporation of $\tau_{ec} = 5\tau_k$ the magnitude of τ_p is reduced to $0.5\tau_k$ by the end of the simulation. As expected, a decrease of the particle time constant results in the decrease of its velocity autocorrelation; the larger the evaporation rate the smaller the velocity autocorrelation at all times.

An important issue to address at this point is the speed of adjustment of the velocity of the evaporating particle to that of its surrounding fluid. As indicated in figure 1 when particles are released with a zero velocity relative to the fluid, there is a time delay before the average particle Reynolds number reaches a stationary value. Therefore, a comparison of the magnitude of $\langle\langle Re_p \rangle\rangle$ of the evaporating particle with those of the stationary non-evaporating particle at the same τ_p provides a reasonable indication of the speed of momentum adjustment. For the highest evaporation rate ($\tau_{ec} = 5\tau_k$) shown in figure 5, $\langle\langle Re_p \rangle\rangle$ ($\tau_p = 3\tau_k$) = 0.585 and $\langle\langle Re_p \rangle\rangle$ ($\tau_p = \tau_k$) = 0.173. These values are very close to those for stationary non-evaporating particles at the same particle time constant (0.589 and 0.172, respectively). This suggests that evaporating particles adjust quickly to their new conditions.

For a constant particle Schmidt number, the rate of evaporation becomes dependent on the magnitude of the particle Reynolds number and is different for each particle. Therefore, even with an identical initial τ_p value, the evaporation process results in polydispersity of drops. The remainder of this section is devoted to the study of the properties of the drop size distributions for different values of the particle time constant, the evaporation rate, and various initial conditions.

Figure 6 shows the temporal evolutions of the probability density function (pdf) of the variable $\tau_p^{1/2}$ (proportional to the particle diameter). In this simulation, $\tau_{p0} = 5\tau_k$, $\tau_{ec} = 5\tau_k$, and $Sc_p = 1.0$.

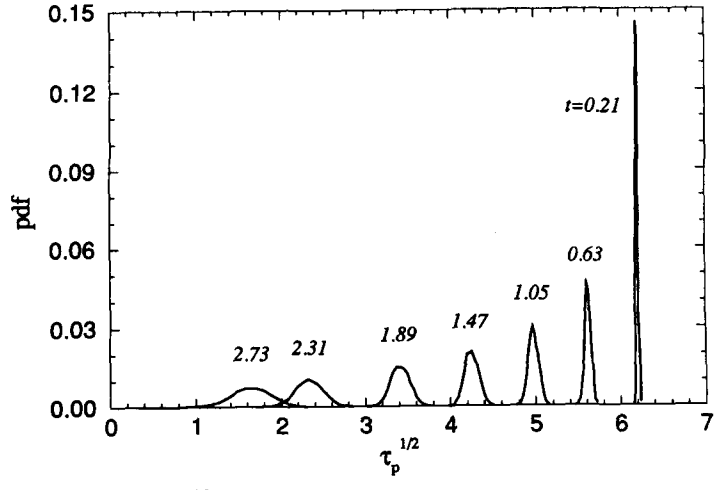

Figure 6. Pdfs of $\tau_p^{1/2}$ at different times for $\tau_{p0} = 5\tau_k$, $\tau_{ec} = 5\tau_k$, and $Sc_p = 1$.

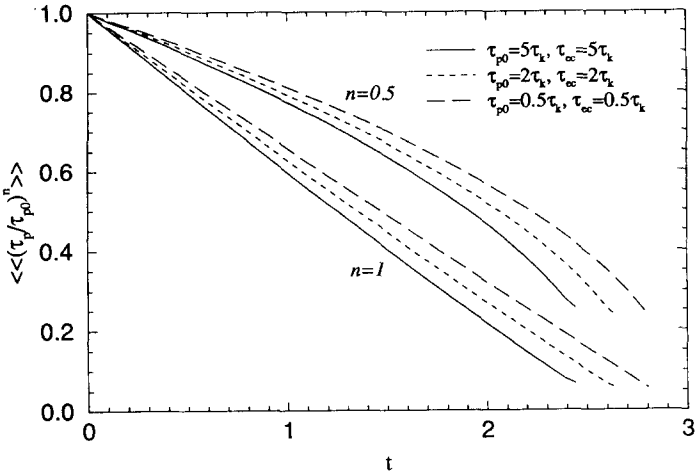

Figure 7. Temporal variations of $\langle\langle \tau_p/\tau_{p0} \rangle\rangle$ and $\langle\langle (\tau_p/\tau_{p0})^{1/2} \rangle\rangle$ for different initial particle time constants and evaporation rates.

The particles start to evaporate from a stationary condition at time $t = 0$, when the pdf is a delta function. At longer times the mean shifts towards smaller $\tau_p^{1/2}$ values due to reduction of the particle size. The variations of $\langle\langle (\tau_p/\tau_{p0})^{1/2} \rangle\rangle$ and $\langle\langle \tau_p/\tau_{p0} \rangle\rangle$ are shown in figure 7 for simulations in which three different groups of particles are considered; $\tau_{p0} = 5\tau_k$, $2\tau_k$, and $0.5\tau_k$ with corresponding initial evaporation rates of $\tau_{ec} = 5\tau_k$, $2\tau_k$, and $0.5\tau_k$, respectively. Equation [5] indicates that for a constant rate of evaporation, τ_p decreases linearly with time. When the evaporation rate is variable, a deviation from the linear behavior is expected. However, figure 7 shows that for the cases considered here the deviation is relatively small. This is mainly due to the one-way coupling assumption. Obviously, larger particles show a more nonlinear behavior than the smaller ones due to their larger Re_p values. The magnitude of the particle diameter decreases nonlinearly from the beginning and the rate of nonlinearity increases with time. This is easily explained by comparing the rate of change of τ_p and $\tau_p^{1/2}$. For a constant rate of change of τ_p (which is a reasonable assumption for the cases considered here), $d(\tau_p^{1/2})/dt \sim \text{constant}/\tau_p^{1/2}$. Therefore, the rate of the diameter decrease becomes larger as the size of the particle is reduced. Notice that although the initial evaporation rate for each group has been chosen proportional to its initial particle time constant, the curves of $\langle\langle (\tau_p/\tau_{p0})^{1/2} \rangle\rangle$ and $\langle\langle \tau_p/\tau_{p0} \rangle\rangle$ for different groups of particles are not identical. This is due to the nonlinear variation of Re_p with τ_p as observed in figure 1. When τ_p is increased by a factor of 10, the corresponding $\langle\langle Re_p \rangle\rangle$ is increased by a factor of about 15.

Shortly after the onset of evaporation, a wide range of droplet sizes is observed. In figure 8 the pdfs of $\tau_p^{1/2}$ are considered at an intermediate time ($t = 1$) and are shown to be close to Gaussian for all the cases. In figure 9 the temporal variations of the skewness and the kurtosis of the pdfs for the three cases are considered. At short times the pdfs are skewed towards the smaller sizes while at intermediate times they become more symmetric. Although the differences in Re_p for the particles is responsible for the generation of size distribution at each time, the mechanism which results in variation of Re_p is different at short and at long times. At short times, the diameters of all the particles are approximately the same and the changes in Re_p are due to the differences in the spatial locations of the particles. At long times, the differences in Re_p are also dependent on the size variations. In general, at intermediate times the pdf of the particle size is approximately Gaussian. However, the larger the initial particle time constant, the closer the pdf is to Gaussian. This is evident from figure 9 that shows larger deviations from Gaussian skewness and kurtosis values as the initial size of the particles is decreased. Larger particles with $\tau_{p0} = 5\tau_k$ and $2\tau_k$ attain pdfs with slightly positive skewness after about one eddy turnover time. The skewness of the particles with $\tau_{p0} = 0.5\tau_k$ remains negative for the entire simulation. In general, for large particles, after an initial transient time which depends on the particle size the pdfs become very close to Gaussian. But near the end of the simulations again the pdfs start to deviate from Gaussian. In fact, when the skewness and the kurtosis of different cases are plotted versus the instantaneous

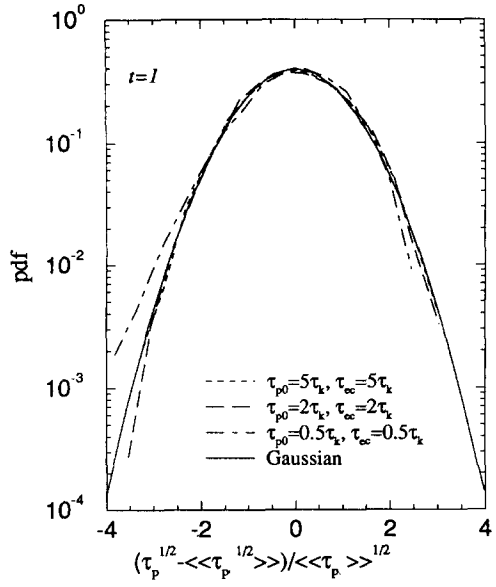

Figure 8. Normalized pdfs of $\tau_p^{1/2}$ for different particle time constants and evaporation rates at $t = 1$.

mean particle time constant, the pdfs become more non-Gaussian as $\langle\langle\tau_p\rangle\rangle$ becomes smaller than τ_k. This is due to nonlinearity of the rate of decrease of $\tau_p^{1/2}$ at small particle time constants. As indicated above, as the size of the drop decreases, the rate of change of its diameter increases and figure 7 shows that this effect is more pronounced when the drop time constant is small. Therefore, the diameters of the smaller drops decrease faster than the diameters of the larger drops and the pdf becomes skewed towards smaller diameter values.

We now consider the pdfs of particles with different initial evaporation rates. In figure 10 the temporal variations of the skewness and kurtosis for particles with $\tau_{p0} = 5\tau_k$ and initial evaporation rates of $\tau_{ec} = 5\tau_k$, $2.5\tau_k$, τ_k, and $0.4\tau_k$ are presented. The initial condition for these particles is different than those considered earlier. At $t = 0$ the particles are released with a zero velocity relative to the local fluid particle. An initial transient time is needed before the particles attain momentum equilibrium with the flow. Figure 10 indicates that this initial transient time appears independent of the rate of evaporation and is about the same as that required by the non-evaporating particles with $\tau_p = 5\tau_k$ to reach the stationary condition (cf. figure 1). After the momentum equilibrium is reached, the pdfs of $\tau_p^{1/2}$ tend to become Gaussian. Towards the end of the simulation, the pdfs for cases with higher evaporation rates ($\tau_{ec} = 5\tau_k$ and $\tau_{ec} = 2.5\tau_k$) become

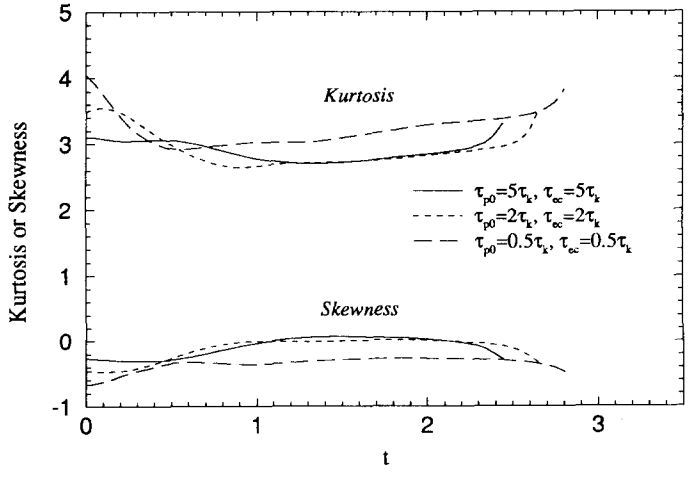

Figure 9. Temporal variations of the kurtosis and skewness of $\tau_p^{1/2}$.

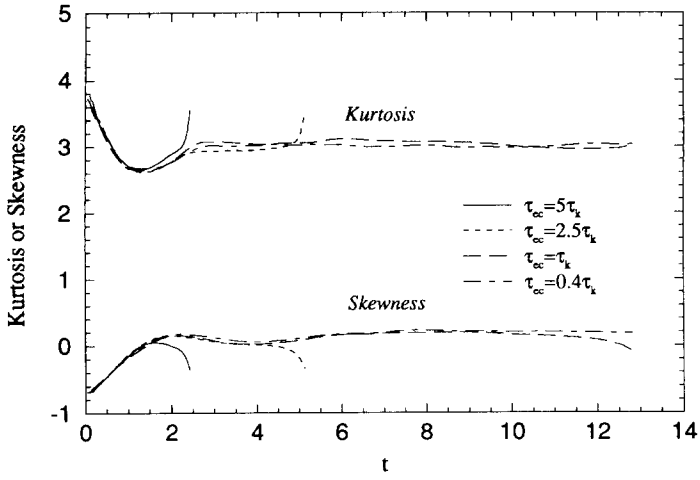

Figure 10. Temporal variation of the kurtosis and skewness of $\tau_p^{1/2}$ for an initial particle time constant $\tau_{p0} = 5\tau_k$ at different evaporation rates.

strongly non-Gaussian. However, as the evaporation rate decreases the pdfs tend to remain Gaussian. This is due to the smaller $\tau_p^{1/2}$ variances for cases with smaller evaporation rates. Therefore, as the evaporation rate is decreased a "narrower" pdf is obtained and the difference between the diameters of different drops is decreased. This, in turn, diminishes the effect of the nonlinearity of the rate of change of diameter which tends to skew the pdfs.

Effect of particle Schmidt number. The magnitude of the particle Schmidt number influences the rate of evaporation as indicated by [4]. Figure 11 shows the temporal variation of the Lagrangian average of the nonlinear part of [4] for two different particle time constants and three Sc_p values. Two different initial conditions are considered: stationary (solid symbols) and non-stationary (hollow symbols). In non-stationary cases, the initial particle velocity is zero relative to the local fluid; therefore, the initial value of $\langle\langle C_{Re} - 1 \rangle\rangle$ is zero. After an initial increase, this value starts to decrease due to the decrease of the particle size and consequently the decrease of the particle Reynolds number. The comparison of the results in the stationary and the non-stationary cases at the same $Sc_p = 1$ reveals that for large particles, the value of $\langle\langle C_{Re} - 1 \rangle\rangle$ in the non-stationary case overshoots that in the stationary case. This is due to the variation of Re_p in time which experiences an overshoot before it reaches a stationary value (figure 1). For small particles Re_p does not overshoot, and neither does $\langle\langle C_{Re} - 1 \rangle\rangle$. In general, the increase of Sc_p enhances the contribution of the nonlinear part of [4]; however, for the cases considered here with Sc_p as large as 5 this contribution is always less than 50% of the constant evaporation rate ($\langle\langle C_{Re} - 1 \rangle\rangle < 0.5$).

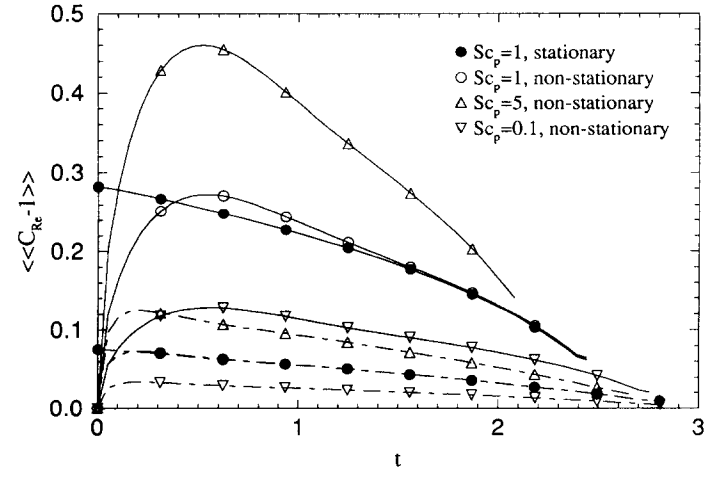

Figure 11. Variation of $\langle\langle C_{Re} - 1 \rangle\rangle$ with time. (—) $\tau_{p0} = 5\tau_k$, $\tau_{cc} = 5\tau_k$; (- · · · -), $\tau_{p0} = 0.5\tau_k$, $\tau_{cc} = 0.5\tau_k$.

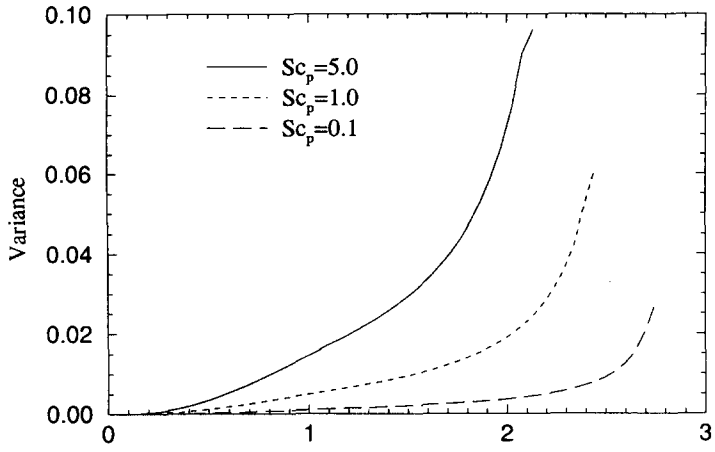

Figure 12. Temporal variations of the variance of $\tau_p^{1/2}$. $\tau_{p0} = 5\tau_k$, $\tau_{ec} = \tau_k$.

In figure 12 the temporal evolution of the variance of $\tau_p^{1/2}$ is shown for three different particle Schmidt numbers. The initial particle time constant is $\tau_{p0} = 5\tau_k$ for all cases. As the particle Schmidt number increases the variance also increases. This means that at larger Sc_p, a wider range of particle sizes are present. At $Sc_p = 5\tau_k$ the difference between the maximum and the minimum values at the end of the simulation is about 0.41 while the corresponding difference for $Sc_p = 0.1$ is about 0.24. Therefore, while the minimum value of $(\tau_p/\tau_{p0})^{1/2}$ at the end of the simulation is the same for both cases, the case with the higher Sc_p value contains a higher number of larger particles. This is due to the fact that the increase of Sc_p enhances the effect of Re_p on evaporation. The skewness of the particle distribution towards smaller particles is also evident by comparing the distance from the mean value to the minimum and the maximum value at all times. Examination of the temporal variations of the skewness of $\tau_p^{1/2}$ revealed that, in all the cases, the skewness takes negative values at small times and then increases with time. For large τ_{p0} values, the skewness reaches small positive values for intermediate times. But it decreases and takes negative values close to the end of the simulation when τ_p values for most of the particles become small. Particles with smaller τ_{p0} values, have negative skewness during the entire simulation. In general, the effect of the particle time constant is more significant than the particle Schmidt number on the skewness of the particle sizes.

Effect of spray size. In many practical applications the size of the spray is smaller than the characteristic size of the flow. As the spray evolves with flow, dispersion of the particles is strongly affected by the interactions between the spray and the carrier fluid. It is expected that the size of the spray relative to the characteristic length scale of turbulence plays an important role on dispersion. In the case of evaporating particles this becomes even more important since the size distribution is also directly affected by the interaction between the droplets and the flow at different scales. In this subsection we investigate the effect of the relative size of the spray on the particle size distribution. We initialize the problem by randomly distributing the particles inside a cubic box which is located at the center of the computational box. All particles have the same size and a zero velocity relative to the local fluid element at $t = 0$. The length of one side of the particle-containing box is denoted by S and indicates the spray size.

First we consider a case with initial spray size $S_0/l = 0.28$. In figure 13 the variations of the kurtosis and skewness of $\tau_p^{1/2}$ are shown for two different initial particle time constants. On the same figures the temporal variations of the spray size are also shown. This size is determined by the dimension of the smallest box containing all of the particles at any time. Figure 13 reveals that the kurtosis and skewness of the particle size are very different from those corresponding to Gaussian. In contrast to the cases discussed earlier, the skewness is positive throughout the simulation. For both of the particle time constants considered, the growth of the spray size is nearly linear in time. This can be interpreted as a constant diffusion velocity which is about the same in both cases. The normalized spray size increases from its initial value to a final value corresponding to the ratio of the computational box to the integral length scale.

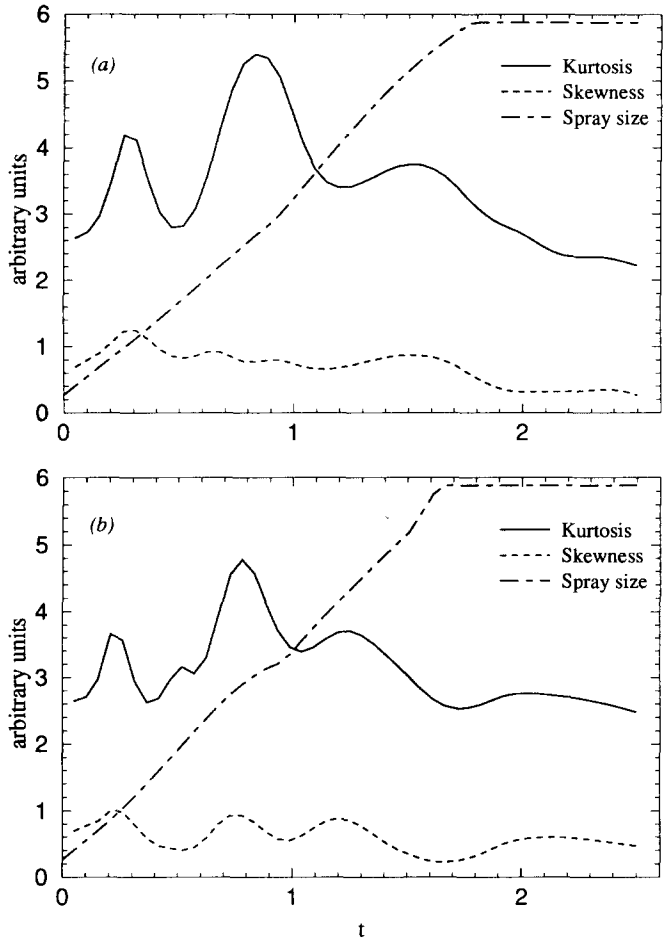

Figure 13. Temporal variations of the kurtosis and skewness of $\tau_p^{1/2}$, and spray size for $Sc_p = 1$ and $S_0/l = 0.28$. (a) $\tau_{p0} = 5\tau_k$ and $\tau_{cc} = 5\tau_k$, (b) $\tau_{p0} = 0.5\tau_k$ and $\tau_{cc} = 0.5\tau_k$.

Next, we consider cases with different S_0/l values. Examination of the temporal variations of the kurtosis and skewness of $\tau_p^{1/2}$ for cases with different S_0 and τ_{p0} values revealed that as the initial spray size is increased, the oscillations in the skewness and the kurtosis diminish and the values

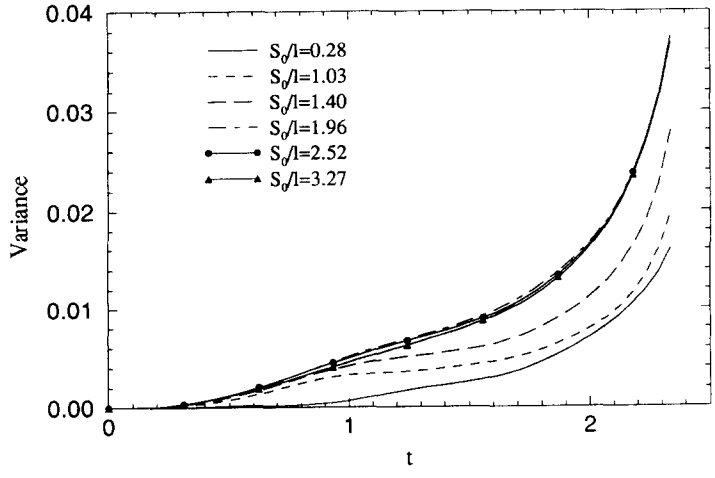

Figure 14. Temporal variation of the variance of $\tau_p^{1/2}$ for different initial spray sizes. $\tau_{p0} = 5\tau_k$, $\tau_{cc} = 5\tau_k$ and $Sc_p = 1$.

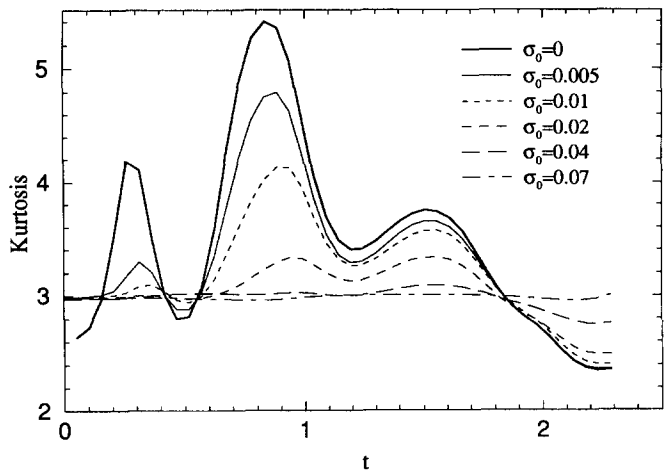

Figure 15. Temporal variation of the kurtosis of $\tau_p^{1/2}$ for different values of the initial standard deviation. $\tau_{p0} = 5\tau_k$, $\tau_{ec} = 5\tau_k$ and $S_0/l = 0.28$.

approach those corresponding to the Gaussian distribution. Figure 14 shows the time variation of the variance of $\tau_p^{1/2}$ for several values of S_0/l. The initial particle time constant and the evaporation rate are $\tau_{p0} = 5\tau_k$ and $\tau_{ec} = 5\tau_k$, respectively. As the initial spray size is increased, the instantaneous rate of variance increase approaches an asymptotic value corresponding to the case with $S_0/l = 1.96$. This implies that if the initial spray size is larger than about twice the integral length scale, the effect of the spray size on the variance is negligible. In general, three distinct regions are observed on the curves shown in figure 14. The first region corresponds to initial times $0 < t < 0.3$ during which the rate of variance growth is very small. Since particles are released with zero relative velocity, they have the same initial Re_p values and consequently the same initial evaporation rate. Therefore, at initial times the variance remains close to zero. As the particle Reynolds number increases, the particles experience different evaporation rates and the variance starts to increase. Figure 11 shows that the time interval $0 < t < 0.3$ corresponds to the period during which $\langle\langle C_{Re} \rangle\rangle$ adopts large values. At large particle Reynolds numbers, in the second region of the curves of figure 14 ($0.3 < t < 2$), the variance grows with a larger rate. The third region ($t > 2$) is marked by the largest rate of variance growth. This is explained by considering figure 7 which shows that the rate of reduction of $\tau_p^{1/2}$ increases at large times when the size of the particles is small.

Effect of the initial particle size distribution. The observed deviations of the particle size pdfs from the Gaussian for small S_0/l values motivate the analysis of cases with initial Gaussian diameter pdfs. These cases are characterized by the initial standard deviation of $\tau_p^{1/2}$ denoted by σ_0. The cases considered in previous subsections refer to $\sigma_0 = 0$. The velocity and the position of the particles are initialized randomly similar to previous cases. The size of each particle is selected randomly from a Gaussian seed with specified values for the mean and the standard deviation. In order to prevent very small and very large particle time constants, the standard deviations considered are relatively small.

Figure 15 shows the kurtosis of $\tau_p^{1/2}$ for cases with several values of the initial standard deviation. The initial mean particle time constant is $\langle\langle \tau_{p0} \rangle\rangle = 5\tau_k$. The case with the smallest initial spray size ($S_0/l = 0.28$) is considered as the pdfs for this case deviate more from Gaussian; therefore, the effects of the initial size distribution are amplified. As expected, by increasing the initial standard deviation, the pdf becomes closer to Gaussian. For the range of $\langle\langle \tau_{p0} \rangle\rangle$ and S_0/l values considered here, a nearly perfect Gaussian pdf is achieved when the initial standard deviation is $\sigma_0 = 0.07$. The effect of the initial standard deviation is more pronounced at early times. An interesting feature observed in figure 15 is the similarity of the oscillations of the kurtosis curves for different cases. This verifies our previous observation in that these oscillations are due to interactions between the particles and the large structures of the flow. Since the initial spray size is identical, a similar oscillation pattern is experienced in all the cases.

Next, we consider the effect of the initial spray size for a constant initial standard deviation of

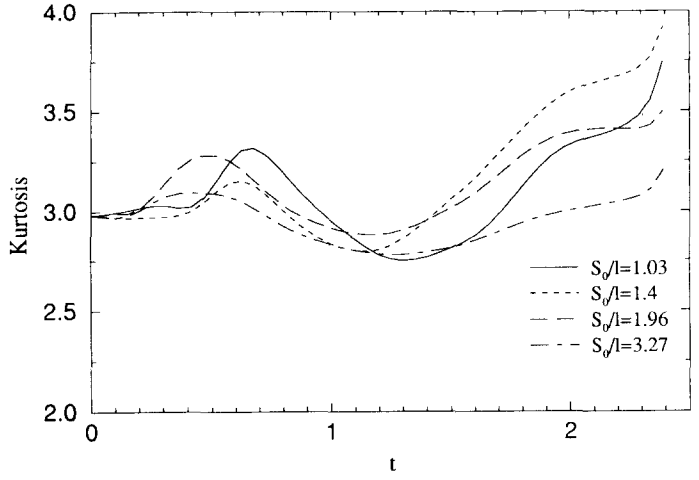

Figure 16. Temporal variation of the kurtosis of $\tau_p^{1/2}$ for different initial spray sizes. $\tau_{p0} = 5\tau_k$, $\tau_{ec} = 5\tau_k$ and $\sigma_0 = 0.02$.

$\sigma_0 = 0.02$. Figure 16 shows the temporal variation of the kurtosis of $\tau_p^{1/2}$. Similarly to the cases with $\sigma_0 = 0$, the pdf becomes more Gaussian as the initial spray size increases. Contrary to the cases with the same S_0/l, the kurtosis curves of figure 16 are not similar. The time of the occurrence of the first peak is decreased as the initial spray size is increased. This again is due to the interaction of the spray with the larger scales of the flow as the spray size increases. The examination of the variance of $\tau_p^{1/2}$ (not shown) for different cases indicated that the variance curves collapse for $S_0/l \geqslant 1.4$ when $\sigma_0 = 0.02$ in contrast to $S_0/l \geqslant 1.96$ when $\sigma_0 = 0$.

Finally, for completion, several cases are considered with initially non-Gaussian drop size distributions. For these cases, the initial distribution consists of two distinct uniform-size groups of drops (the initial pdf of $\tau_p^{1/2}$ is a double delta). The drops are initially injected into the flow with zero velocity relative to the local fluid and $Sc_p = 1$. Figure 17 shows the temporal evolution of the pdf of $\tau_p^{1/2}$ for a case with $\langle\langle \tau_{p0} \rangle\rangle = 5\tau_k$ and $\sigma_0 = 0.128$. As indicated in the figure, by the time $t = 0.52$ the two initially segregated branches of the pdf start to merge resulting in the increase of the $\tau_p^{1/2}$ kurtosis (figure 18). At $t \simeq 2.35$ the double-hump pdf evolves into a single peak one; at the final time ($t = 2.62$), the pdf is close to Gaussian. However, it is also possible that with a large initial separation between the drop time constants (large σ_0) a single-hump pdf is not attained during the evaporation period. Figure 18 shows that as $\langle\langle \tau_{p0} \rangle\rangle$ is increased, for the same σ_0, the kurtosis of $\tau_p^{1/2}$ deviates less from that of Gaussian. Inspection of the pdf evolution for the case with $\langle\langle \tau_{p0} \rangle\rangle = 1$

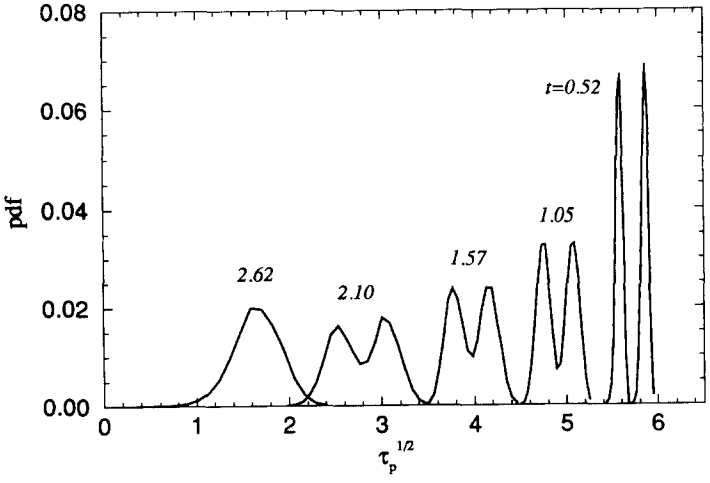

Figure 17. Pdfs of $\tau_p^{1/2}$ at different times. The initial pdf is double delta with drop time constants at $4.8\tau_k$ and $5.2\tau_k$. $\tau_{ec} = 5\tau_k$ and $Sc_p = 1$.

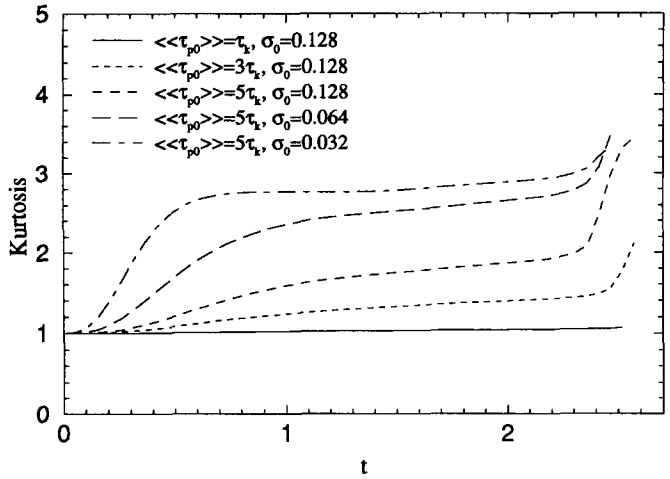

Figure 18. Temporal variation of the kurtosis of $\tau_p^{1/2}$ for different initial mean drop time constants and initial standard deviations.

(not shown) indicates the persistence of the double-hump pdf throughout the simulation. The effect of the variation of the initial standard deviation on the kurtosis is also shown in figure 18 for pdfs with $\langle\langle\tau_{p0}\rangle\rangle = 5\tau_k$. As expected, the evolution from a double-hump pdf into one with a single-hump is expedited with the decrease of σ_0.

Based on these results, it is concluded that the evolution of the pdf is very sensitive to several parameters, especially $\langle\langle\tau_{p0}\rangle\rangle$, τ_{ec}, σ_0, and S_0/l. Based on the magnitudes of these parameters and the initial form of the pdf, several asymptotic ($\langle\langle\tau_p\rangle\rangle \to 0$) forms of the pdf are produced. It would be instructive to suggest a dynamic (or Langevin) equation governing the evolution of the dispersed phase pdfs in a carrier gas with a Gaussian velocity field. This equation must include the parameters identified here as model input. Construction of such a stochastic model is currently underway; the DNS results produced here are very useful in appraising the performance of such models.

4. SUMMARY AND CONCLUDING REMARKS

Results obtained by direct numerical simulation (DNS) are used to investigate dispersion of both non-evaporating and evaporating particles in dilute stationary isotropic incompressible turbulent flow. The evaporating case is considered with both constant and variable rates of evaporation. In the simulations of non-evaporating particles, the effects of the particle time constant and the drift velocity on the particle autocorrelation, turbulence intensity and diffusivity are investigated. In agreement with the results of previous studies, it is found that the increase of the particle time constant results in the increase of the particle velocity autocorrelation and the decrease of its turbulence intensity. There is good agreement between the DNS results and the model of Mei *et al.* (1991) for the ratio of the particle turbulence intensity to the carrier fluid turbulence intensity, in the absence of gravity. But the agreement diminishes as the value of the drift velocity is increased. The particle turbulent diffusivity is rather insensitive to the changes in the particle time constant in accord with the experiment of Wells and Stock (1983). However, the present results exhibit a peak value in the variation of the particle turbulence diffusivity with the particle time constant. In the absence of gravity, the peak value occurs for particle time constants comparable to the Kolmogorov time scale. In the presence of gravity, the peak value for the particle diffusivity is observed in the direction normal to the gravity direction. The value of the particle time constant at which the peak value occurs depends on the magnitude of the drift velocity. No apparent peak value is observed for the particle diffusivity in the gravity direction. In general, the particle diffusivity is very sensitive to the drift velocity.

The effects of the constant rate evaporation on the particle velocity autocorrelation are studied for different initial particle time constants. The results show a decrease of the particle velocity autocorrelation with the increase of the evaporation rate for all the values of the initial particle

time constant. Variable rate evaporation results in polydispersity of drops. The effects of the initial drop time constant, the initial evaporation rate, and the drop Schmidt number on the probability density function (pdf) of the drop size are studied. Both cases with initially stationary and non-stationary particle velocities are considered. For cases with initially identical particle sizes it is found that after an initial transient period, the pdf of the particle size becomes Gaussian. The behavior of the pdf at long times depends on the particle size and the evaporation rate. In general, when the mean particle time constant becomes smaller than the Kolmogorov time scale, the pdf of the particle size starts to deviate from Gaussian. The extent of this deviation decreases with the decrease of the evaporation rate. The simulated results with different particle Schmidt numbers indicate an increase of the variance of $\tau_p^{1/2}$ with the increase of the Schmidt number. Also, the results show that the particle time constant is more influential than the particle Schmidt number in affecting the skewness of the particle sizes.

The effects of the initial spray size on the distribution of the particle size are also studied. The results indicate significant deviations from Gaussian when the initial spray size is smaller than the flow integral length scale. The spray size displays a linear temporal growth which is indicative of a constant rate of diffusion. This rate appears to be approximately the same for all the cases considered here. In addition to the initially identical particle sizes, several cases are considered in which the initial sizes of the particles are selected from a Gaussian seed. For an initial constant spray size (0.28 times the flow integral scale) it is shown that a nearly perfect Gaussian behavior is achieved when the standard deviation of the initial particle size distribution is 0.07. This value changes with the initial mean particle time constant and the initial spray size. For an initial double-delta pdf of the drop size it is shown that a transition to Gaussian pdf is possible provided that the initial mean drop time constant is large and/or the initial standard deviation is small.

At this point it is emphasized that the results presented here are based on simulations with several assumptions and simplifications as stated in section 2. These were necessary to make the problem computationally tractable with available resources. Some of these assumptions can be relaxed with improved computational capabilities. Future work is recommended in DNS of evaporating drop dispersion with two-way coupling, inclusion of compressibility effects, and modification of some of the coupling relations. It is also recommended to perform simulations with larger resolutions/realizations with data analysis coupled with consideration of preferential distribution of particles. The results generated thus far elucidate many important issues in regard to complex physics of drop dispersion in turbulent flows. These results motivate further extensions and utilizations of DNS for the analysis of more complex multiphase turbulent reacting flow systems.

Acknowledgements—We are grateful to Professor R. Mei for providing the data used in figure 3. This work is sponsored by the U.S. Office of Naval Research under Grant N00014-94-10667. Computational resources are provided by the SEAS Computing Center at SUNY—Buffalo and by the NCSA Facilities at the University of Illinois at Urbana—Champaign.

REFERENCES

Chao, B. T. (1964) Turbulent transport behavior of small particles in dilute suspension. *Osterreichisces Ingenieur-Archiv*. **18,** 7–21.

Csanady, G. T. (1963) Turbulent diffusion of heavy particles in the atmosphere. *J. Atmos. Sci.* **20,** 201–208.

Eaton, J. K. and Fessler, J. R. (1994) Preferential concentration of particles by turbulence. *Int. J. Multiphase Flow Suppl.* **20,** 169–209.

Elghobashi, S. and Truesdell, G. C. (1992) Direct simulation of particle dispersion in a decaying isotropic turbulence. *J. Fluid Mech.* **242,** 655–700.

Elghobashi, S. and Truesdell, G. C. (1993) On the two-way interaction between homogeneous turbulence and dispersed solid particles. I: Turbulence modification. *Phys. Fluids* **5,** 1790–1801.

Givi, P. (1989) Model free simulations of turbulent reactive flows. *Prog. Energy Combust. Sci.* **15,** 1–107.

Givi, P. and Madnia, C. K. (1993) Spectral methods in combustion. In *Numerical Modeling in*

Combustion, ed. by T. J. Chung, Chapter 8, pp. 409–452. Taylor and Francis, Washington, D.C.

Hinze, J. O. (1975) *Turbulence*. McGraw-Hill Book Company, New York.

Kraichnan, R. H. (1970) Diffusion by a random velocity field. *Phys. Fluids* **13,** 22–31.

Maxey, M. R. and Riley, J. J. (1983) Equation of motion for a small rigid sphere in a nonuniform flow. *Phys. Fluids* **26,** 883–889.

McLaughlin, J. B. (1989) Aerosol particle deposition in numerically simulated channel flow. *Phys. Fluids* **1,** 1211–1224.

McLaughlin, J. B. (1994) Numerical computation of particles–turbulence interaction. *Int. J. Multiphase Flow Suppl.* **20,** 211–232.

Mei, R., Adrian, R. J. and Hanratty, T. J. (1991) Particle dispersion in isotropic turbulence under Stokes drag and basset force with gravitational settling. *J. Fluid Mech.* **225,** 481–495.

Nguyen, Q-V., Rangel, R. H. and Dunn-Rankin, D. (1991) Measurement and prediction of trajectories and collision of droplets. *Int. J. Multiphase Flow* **17,** 159–177.

Pismen, L. M. and Nir, A. (1978) On the motion of suspended particles in stationary homogeneous turbulence. *J. Fluid Mech.* **84,** 193–206.

Ranz, W. E. and Marshall, W. R. (1952) Evaporation from drops. *Chem. Engng Prog.* **48,** 141–173.

Reeks, M. W. (1971) On the dispersion of small particles suspended in an isotropic turbulent fluid. *J. Fluid Mech.* **83,** 529–546.

Riley, J. J. and Patterson, G. S. (1974) Diffusion experiments with numerically integrated isotropic turbulence. *Phys. Fluids* **17,** 292–297.

Shearer, A. J., Tamura, H. and Faeth, G. M. (1979) Evaluation of locally homogeneous flow model of spray evaporation. *J. Energy* **3,** 271–278.

Snyder, W. H. and Lumley, J. L. (1971) Some measurements of particle velocity autocorrelation functions in a turbulent flow. *J. Fluid Mech.* **48,** 41–47.

Solomon, A. S. P., Shuen, J-S., Zhang, Q-F. and Faeth, G. M. (1984) A theoretical and experimental study of turbulent evaporating sprays. NASA CR 174760.

Spalding, D. B. (1953) The combustion of liquid fuels. In *Proceedings of 4th Symp. (Int.) on Combustion*, pp. 847–864. The Combustion Institute, Baltimore, MD.

Squires, K. D. and Eaton, J. K. (1990) Particle response and turbulence modification in isotropic turbulence. *Phys. Fluids* **2,** 1191–1203.

Squires, K. D. and Eaton, J. K. (1991a) Measurements of particle dispersion obtained from direct numerical simulations of isotropic turbulence. *J. Fluid Mech.* **226,** 1–35.

Squires, K. D. and Eaton, J. K. (1991b) Preferential concentration of particles by turbulence. *Phys. Fluids* **3,** 1169–1178.

Strehlow, R. A. (1985) *Combustion Fundamentals*. McGraw-Hill, New York.

Tchen, C. M. (1947) Turbulent reacting flows. Ph.D. thesis, Delft University, The Hague.

Truesdell, G. C. and Elghobashi, S. (1994) On the two-way interaction between homogeneous turbulence and dispersed solid particles. II: Particle dispersion. *Phys. Fluids* **6,** 1790–1801.

Wang, L-P. and Maxey, M. R. (1993) Settling velocity and concentration distribution of heavy particles in isotropic turbulence. *J. Fluid Mech.* **256,** 27–68.

Wells, M. R. and Stock, D. E. (1983) The effects of crossing trajectories on the dispersion of particles in a turbulent flow. *J. Fluid Mech.* **136,** 31–62.

Wen, F., Kamalu, N., Chung, J. N., Crowe, C. T., and Troutt, T. R. (1992) Particle dispersion by vortex structures in plane mixing layers. *J. Fluids Eng.* **114,** 657–666.

Yudine, M. I. (1959) Physical considerations on heavy-particle diffusion. *Adv. Geophys.* **6,** 185–191.

Zhou, L. X. (1993) *Theory and Numerical Modeling of Turbulent Gas–Particle Flows and Combustion*. CRC Press, FL, USA.